

# IRAM Memo 2025-1

## NOEMA sensitivity estimator

J. Pety<sup>1,2</sup>, J. Boissier<sup>1</sup>, S. Bardeau<sup>1</sup>, E. Reynier<sup>1</sup>

1. IRAM (Grenoble)
2. Observatoire de Paris

Feb, 6<sup>th</sup> 2025  
Version 1.0

### **Abstract**

This memo describes the equations used in the NOEMA sensitivity estimator available on the online sensitivity estimator (<https://oms.iram.fr/tse/>) and used for proposal submission in the Proposal Management System.

This memo is a full rewriting of the older memos dedicated to the subject to consolidate the equations and to take into account the new dual band and frequency cycling modes. The different versions of the memo 2015-2 are only kept in order to know how the sensitivity estimates were done in past proposal sessions.

## Contents

<b>1</b>	<b>NOEMA instrumental modes</b>	<b>3</b>
<b>2</b>	<b>The interferometric point source sensitivity</b>	<b>3</b>
2.1	Power and sensitivity measured at the correlator output for one baseline . . . . .	3
2.2	Quantization efficiency . . . . .	4
2.3	From the temperature power to the flux . . . . .	4
2.4	Collecting the measurements from all baselines . . . . .	4
2.5	Signal decorrelation . . . . .	5
2.6	Noise vs signal . . . . .	5
2.7	Summary and interpretation . . . . .	5
<b>3</b>	<b>The interferometric extended source sensitivity</b>	<b>6</b>
3.1	Yielding the interferometric extended source sensitivity . . . . .	6
3.2	Interpretation . . . . .	7
<b>4</b>	<b>The system temperature</b>	<b>7</b>
4.1	Definition . . . . .	7
4.2	Line vs continuum system temperature . . . . .	7
4.3	Receiver temperature . . . . .	11
<b>5</b>	<b>In practice</b>	<b>11</b>
5.1	Line vs continuum system temperature . . . . .	11
5.2	The number of polarizations . . . . .	12
5.3	Actual computations . . . . .	12
5.4	Elapsed telescope time vs on-source time . . . . .	12
5.5	Sensitivity for a single-source, single-field observations . . . . .	14
5.6	Sensitivity for track-sharing, single-field observations . . . . .	14
5.7	Sensitivity for mosaicking . . . . .	15
<b>6</b>	<b>Acknowledgements</b>	<b>18</b>
<b>A</b>	<b>A few reminders: Flux vs brightness in radio-astronomy</b>	<b>20</b>
A.1	Antenna power pattern, solid angles, associated efficiencies . . . . .	20
A.2	Source and observed flux density . . . . .	20
A.3	Observed brightnesses . . . . .	21
A.4	Basic relation between received spectral power and sky brightness . . . . .	21
A.5	Brightness temperature . . . . .	21
A.5.1	Brightness temperature . . . . .	21
A.5.2	Interpretation . . . . .	22
A.6	Effective aperture and aperture efficiency . . . . .	22
A.7	Relationship between effective aperture and antenna solid angle . . . . .	22
A.7.1	Statement . . . . .	22
A.7.2	Demonstration . . . . .	23
A.7.3	Interpretation . . . . .	23

## 1 NOEMA instrumental modes

The most usual instrumental mode for a radio-interferometer is to observe with a single band of receiver a single LO frequency. This mode will be called “standard” mode hereafter. NOEMA introduces two other possibilities:

**In dual band mode**, two frequencies (one at 3 and one at 1 mm) are observed simultaneously. The beam has thus to be split into two beams with the help of a dichroic. This adds some instrumental noise that we will encode as a higher value of the receiver noise.

As the dichroic can be removed from the optical path when doing single band observations, this receiver noise increases will only happen when the sensitivity estimation is done in dual band mode.

**In frequency cycling mode**, the tuning frequency is regularly cycled between  $n_{\text{freq}}$  predefined values inside the same receiver RF band. This implies that the on-source observing time must be split between the different tuning of the frequency cycling. To do this, the user will have to give the percentage of the time required per tuning. The sum of the percentage will have to be equal to 100%. By default, PMS will divide equally the on-source time between the tunings, but the user will have the possibility to modify this time repartition.

After the setup phase, each cycle observed at a given frequency must be surrounded by gain calibration observations at the same frequency. This means that the observing efficiency decreases with respect to the standard instrumental mode: in practice this is like doubling the number of calibrators, since each calibrator will have to be observed at the 2 frequencies (the frequencies of the previous and of the next cycle, whatever the number of cycles).

These two additional possibilities can in principle be combined during the same observation.

This memo describes how the sensitivity estimator tool used in the Proposal Management System (<https://oms.iram.fr/oms/?pms>) encodes the sensitivity estimation for these three instrumental modes. Sections 2, 3, and 4 first reminds the basic equations used to compute the sensitivity of a radio-interferometer, namely, the interferometric point source and extended sensitivity, as well as the system temperature that characterizes the noise added by the receiver, the telescope optics, and the atmosphere. Section 5 details the actual computation as a function of the observing mode.

## 2 The interferometric point source sensitivity

The interferometric point source sensitivity is defined as the rms noise level that should be observed when an actual point source is observed by an interferometer.

### 2.1 Power and sensitivity measured at the correlator output for one baseline

After the atmospheric calibration that converts the measurement scale from the correlator output (in counts) to the  $T_{\text{A}}^*$  scale, the output of the correlator for one correlation is a power equivalent temperature (in the Rayleigh-Jeans domain), which is sampled at a rate of  $2d\nu$ , where  $d\nu$  is the frequency bandwidth over which the power is measured. As explained in the Sect. 4, the standard deviation of each power measurement is given by the system temperature power ( $T_{\text{sys}}$ ). During the integration time ( $\Delta t$ ),  $2d\nu \Delta t$  independent samples of the signal power are measured to ensure the Nyquist sampling of the signal in the bandwidth  $d\nu$ . The signal power is averaged over these independent samples. The uncertainty on the averaged signal power, named sensitivity ( $\sigma_{\text{K}}$ ), is thus standard deviation of the average or

$$\sigma_{\text{K}} = \frac{T_{\text{sys}}}{\sqrt{2d\nu \Delta t}}. \quad (1)$$

One subtlety is that the system temperature characterize one baseline between, eg., antennas  $i$  and  $j$ . Instead of just  $T_{\text{sys}}$ , we should write in all generality  $T_{\text{sys}}^{ij}$  with

$$T_{\text{sys}}^{ij} = \sqrt{T_{\text{sys}}^i T_{\text{sys}}^j}, \quad (2)$$

where  $T_{\text{sys}}^i$  and  $T_{\text{sys}}^j$  are the single dish system temperature of antenna  $i$  and  $j$ . For simplicity, we will keep the notation  $T_{\text{sys}}$  hereafter.

## 2.2 Quantization efficiency

The Analog-to-Digital-Converter (ADC) will quantize the analog signal on a finite number of bits. This can be seen as an additional source of noise that is modeled as a spectrometer efficiency ( $\eta_{\text{spec}} \leq 1.0$ ) and Eq. 1 becomes

$$\sigma_K = \frac{T_{\text{sys}}}{\eta_{\text{spec}} \sqrt{2} d\nu \Delta t}. \quad (3)$$

## 2.3 From the temperature power to the flux

For a point source, it is more natural to express the signal, and thus the sensitivity, in unit of flux. The flux ( $F$ ) of a point source is linked to its brightness temperature  $T_A^*$  through

$$F = J_{\text{ant}}^{\text{sd}} T_A^* \quad \text{with} \quad J_{\text{ant}}^{\text{sd}} = \frac{2k F_{\text{eff}}}{A_{\text{eff}}}, \quad (4)$$

where  $k$  is the Boltzman constant, and  $A_{\text{eff}}$  is the effective area of the antenna (eq. 3-113 in Kraus, 1982), and  $J_{\text{ant}}^{\text{sd}}$  the conversion factor for a typical interferometer antenna. The effective area depends on the observing wavelength when the surface rms accuracy becomes a significant fraction of the wavelength. For NOEMA, the effective area is close to the antenna geometrical surface at 3 mm but significantly lower than it at 1 mm. Using the same conversion factor for the sensitivity, we yield

$$\sigma_{\text{Jy}} = \frac{J_{\text{ant}}^{\text{sd}} T_{\text{sys}}}{\eta_{\text{spec}} \sqrt{2} d\nu \Delta t}. \quad (5)$$

We have the same subtlety for  $J_{\text{ant}}^{\text{sd}}$  as for  $T_{\text{sys}}$ , ie,  $J_{\text{ant}}^{\text{sd}}$  here characterizes one baseline between, eg., antennas  $i$  and  $j$ . Instead of just  $J_{\text{ant}}^{\text{sd}}$ , we should write in all generality  $J_{\text{ant}}^{\text{sd},ij}$  with

$$J_{\text{ant}}^{\text{sd},ij} = \sqrt{J_{\text{ant}}^{\text{sd},i} J_{\text{ant}}^{\text{sd},j}}, \quad (6)$$

where  $J_{\text{ant}}^{\text{sd},i}$  and  $J_{\text{ant}}^{\text{sd},j}$  are the single dish conversion factors for antenna  $i$  and  $j$ . For simplicity, we will also keep the notation  $J_{\text{ant}}^{\text{sd}}$  hereafter.

## 2.4 Collecting the measurements from all baselines

Assuming that the atmosphere and receiving system is independent of the pairs of antenna considered, the previous equation is valid for any baseline of the interferometer. All the visibilities can be averaged into a single visibility to define the point source signal. This implies that the standard deviation (sensitivity) on the point source signal will be divided by the square root of the number of baselines, i.e., the number of pairs of antennas,  $n_{\text{ant}}(n_{\text{ant}} - 1)/2$ , where  $n_{\text{ant}}$  is the number of antennas. The point source sensitivity is then

$$\sigma_{\text{Jy}} = \frac{\langle J_{\text{ant}}^{\text{sd}} T_{\text{sys}} \rangle}{\eta_{\text{spec}} \sqrt{n_{\text{ant}}(n_{\text{ant}} - 1)} d\nu \Delta t}, \quad (7)$$

where  $\langle J_{\text{ant}}^{\text{sd}} T_{\text{sys}} \rangle$  is the average for the different baseline.

## 2.5 Signal decorrelation

$J_{\text{ant}}^{\text{sd}}$  characterizes the antenna hardware, *i.e.* it assumes perfect atmospheric conditions or the use of autocorrelations, as in single-dish measurements. In interferometric mode, the phase of the turbulent atmosphere above each antenna of a given baseline has a random part that causes an additional “attenuation” of the amplitude of the correlation. A point source of 1 Jy flux will appear as a source of  $\eta_{\text{atm}}$  Jy flux (with  $\eta_{\text{atm}} \leq 1.0$ ), if we only use the  $J_{\text{ant}}^{\text{sd}}$  factor. This is called atmospheric decorrelation and it depends on the weather during the observations.

However, the last calibration step of interferometric data is to measure a point source of known flux to deduce the actual conversion factor,  $J_{\text{ant}}^{\text{int}}$ , taking into account the atmospheric decorrelation that happens during the observations. By definition of  $\eta_{\text{atm}}$ , we yield

$$J_{\text{ant}}^{\text{int}} = \frac{J_{\text{ant}}^{\text{sd}}}{\eta_{\text{atm}}} \quad \text{and} \quad J_{\text{ant}}^{\text{int}} \geq J_{\text{ant}}^{\text{sd}}. \quad (8)$$

It can be shown that  $\eta_{\text{atm}}$  is related to the atmospheric rms phase noise ( $\phi_{\text{rms}}$ ) through

$$\eta_{\text{atm}} = e^{-\frac{\phi_{\text{rms}}^2}{2}} \leq 1.0. \quad (9)$$

## 2.6 Noise vs signal

One subtlety is that the additive noise is unaffected by the atmospheric decorrelation, in contrast with the signal, because thermal noise is a random process as the turbulence phase noise. As the conversion factor,  $J_{\text{ant}}^{\text{int}}$ , is applied to the data that can contain signal as well as noise, any attempt to measure the noise rms on visibilities or imaged data will thus result in a standard deviation larger than the one given in Eq. 7 by a factor  $\eta_{\text{atm}}$ . So when we estimate the noise level of an interferometer, we need to take into account the interferometric conversion factor that depends on the typical weather conditions (*i.e.*, the atmospheric rms phase noise). This gives

$$\sigma_{\text{Jy}} = \frac{\langle J_{\text{ant}}^{\text{int}} T_{\text{sys}} \rangle}{\eta_{\text{spec}} \sqrt{n_{\text{ant}} (n_{\text{ant}} - 1) d\nu \Delta t}}. \quad (10)$$

## 2.7 Summary and interpretation

The point source sensitivity for an interferometric measurement reads

$$\sigma_{\text{Jy}} = \frac{\langle J_{\text{ant}}^{\text{int}} T_{\text{sys}} \rangle}{\eta_{\text{spec}} \sqrt{n_{\text{ant}} (n_{\text{ant}} - 1) d\nu \Delta t}}, \quad \text{with} \quad J_{\text{ant}}^{\text{int}} = \frac{J_{\text{ant}}^{\text{sd}}}{\eta_{\text{atm}}} \quad \text{and} \quad \eta_{\text{atm}} = e^{-\frac{\phi_{\text{rms}}^2}{2}} \leq 1.0, \quad (11)$$

where  $\sigma_{\text{Jy}}$  is the rms noise flux obtained by integration with an interferometer of  $n_{\text{ant}}$  identical antenna during the  $\Delta t$  integration time in a frequency resolution  $d\nu$  with the system temperature,  $T_{\text{sys}}$ .  $J_{\text{ant}}^{\text{int}}$  is the conversion factor of any given interferometer antenna taking into account the typical amount of atmospheric decorrelation,  $\eta_{\text{atm}}$ , at the observed wavelength. The product  $J_{\text{ant}}^{\text{int}} T_{\text{sys}}$  is averaged over all independent baselines.

Equation 11 is true only when the source is unresolved, *i.e.*, there is no effect of beam dilution. In practice this is rarely the case because the interferometer tries to resolve the source. Thus, this noise formula should be used with caution when preparing the observations. In practice, this formula is useful when one wishes to compare the sensitivity of two different interferometer. Indeed, this point source sensitivity is independent of the interferometer synthesized beam that depends on the details of the observations and, in particular, the interferometer configuration and the completeness of the Earth synthesis.

### 3 The interferometric extended source sensitivity

The name of interferometric “extended” source sensitivity can be misleading. Indeed, the notion of noise for an extended source depends on the source shape. For instance, a flat source of infinite extent would be measured through the visibility exactly located the phase center, and all other visibilities would only show noise. In this thought experiment the noise level on the constant brightness would thus be the noise of a single visibility! More generally, if we take a Gaussian source of a given FWHM, only the visibilities located inside a  $uv$  radius of a few time  $\lambda/\text{FWHM}$  would contribute to the flux measurement of that Gaussian, and the other visibilities would just be noise.

So the only well defined “extended” source sensitivity is the sensitivity for a source that exactly fills the Gaussian synthesized beam. This is what we will derive in this section.

#### 3.1 Yielding the interferometric extended source sensitivity

The point source sensitivity is well adapted to unresolved sources because it directly delivers the estimation of the flux of these sources. For extended sources, the point source sensitivity that is expressed in unit of Jy/Beam, is difficult to understand because it depends on the synthesized beam resolution in a non-trivial way. When a source is resolved (extended compared to the expected synthesized beam), it is much easier to think in temperature brightness. We thus convert back to a brightness temperature scale, but we now do it at the synthesized beam resolution.

In order to generalize Eq. 4 to the final product of an interferometer, we use the fact (see Sect. A.7) that the beam area ( $\Omega_{\text{ant}}$ ) of a telescope of effective collecting surface  $A_{\text{eff}}$  is linked to the observing wavelength ( $\lambda$ ) through

$$\Omega_{\text{ant}} A_{\text{eff}} = \lambda^2. \quad (12)$$

This yields

$$F = J_{\text{ant}} T_{\text{A}}^* \quad \text{with} \quad J_{\text{ant}} = \frac{2k \Omega_{\text{ant}} F_{\text{eff}}}{\lambda^2}. \quad (13)$$

We will use this relation twice.

- On one hand, we have to use the solid angle of the primary beam  $\Omega_{\text{prim}}$  for  $J_{\text{ant}}^{\text{sd}}$  and  $J_{\text{ant}}^{\text{int}}$ . Noting that this beam area corresponds to the main beam area of each telescope, this yields

$$J_{\text{ant}}^{\text{int}} = \frac{J_{\text{ant}}^{\text{sd}}}{\eta_{\text{atm}}} = \frac{1}{\eta_{\text{atm}}} \frac{F_{\text{eff}}}{B_{\text{eff}}} \frac{2k \Omega_{\text{prim}}}{\lambda^2}. \quad (14)$$

- On the other hand, we have to use the solid angle of the synthesized beam  $\Omega_{\text{syn}}$  for the conversion factor that we have to apply to the deconvolved product ( $J_{\text{ant}}^{\text{syn}}$ ). After calibration (including the impact of the atmospheric decorrelation), imaging, and deconvolution (including a potential phase self-calibration), an interferometer mimick the observation by a **perfect** telescope of angular resolution equal to the synthesized beam. In this case, the beam area is equal to the main beam solid angle (i.e., the interferometric beam efficiency is equal to unity or  $B_{\text{eff}}^{\text{int}} = 1$ ), and to the forward beam solid angle (i.e.,  $F_{\text{eff}}^{\text{int}} = 1$ ). We thus yield

$$J_{\text{ant}}^{\text{syn}} = \frac{2k \Omega_{\text{syn}}}{\lambda^2}. \quad (15)$$

Note that we don’t use the decorrelation efficiency in the later equation. This is also due to the fact that after the data reduction, the deconvolved product should appear as if it was observed by a perfect antenna whose response is exactly a Gaussian of angular size  $\Omega_{\text{syn}}$ .

Combining Eq. 11, 14, and 15, we yield the usual

$$\sigma_{\text{K}} = \frac{\sigma_{\text{Jy}}}{J_{\text{ant}}^{\text{syn}}} \quad \text{with} \quad J_{\text{ant}}^{\text{syn}} = \frac{2\pi k \theta_{\text{maj}} \theta_{\text{min}}}{4 \ln 2 \lambda^2}, \quad (16)$$

which can be rewritten as

$$\sigma_K = \frac{\Omega_{\text{prim}}}{\Omega_{\text{syn}}} \left\langle \frac{F_{\text{eff}} T_{\text{sys}}}{B_{\text{eff}} \eta_{\text{atm}}} \right\rangle \frac{1}{\eta_{\text{spec}} \sqrt{n_{\text{ant}} (n_{\text{ant}} - 1) d\nu \Delta t}} = \frac{\theta_{\text{prim}}^2}{\theta_{\text{maj}} \theta_{\text{min}}} \left\langle \frac{F_{\text{eff}} T_{\text{sys}}}{B_{\text{eff}} \eta_{\text{atm}}} \right\rangle \frac{1}{\eta_{\text{spec}} \sqrt{n_{\text{ant}} (n_{\text{ant}} - 1) d\nu \Delta t}}, \quad (17)$$

where  $\sigma_K$  is the rms noise brightness,  $\theta_{\text{prim}}$  the half primary beam width, and  $\theta_{\text{maj}}$  and  $\theta_{\text{min}}$  the half beamwidth along the major and minor axes of the synthesized beam.

### 3.2 Interpretation

Equation 17 clearly states that the sensitivity to extended sources depends on the dilution of the synthesized beam in the primary beam. This is why this formulation of the sensitivity is well adapted to resolved sources.

For a given interferometer, the primary beamwidth is a fixed quantity while the synthesized beam is to first order proportional to the longest baseline in the current interferometer configuration. Hence, doubling the largest baseline will multiply  $\sigma_K$  by a factor 4 ( $= 2^2$ ) for the same integration time or it will multiply the integration time by a factor 16 ( $= 2^4$ ) in order to reach the same sensitivity. This just reflects that while the interferometer tries to mimic a single-dish antenna of same diameter as the largest baseline, all the antenna of the interferometer only fill a fraction of the total collecting area of the single-dish, this fractions decreasing with a power of two as the baseline linearly increases.

## 4 The system temperature

### 4.1 Definition

The system temperature is a summary of the noise added by the system. This noise comes from 1) the receiver and the optics, 2) the emission of the sky, and 3) the emission picked up by the secondary side lobes of the telescope. It is usual to approximate it (in the  $T_A^*$  scale) with

$$T_{\text{sys}} = \frac{(1 + G_{\text{im}}) \exp \{\tau_s A\}}{F_{\text{eff}}} [F_{\text{eff}} T_{\text{atm}} (1 - \exp \{-\tau_s A\}) + (1 - F_{\text{eff}}) T_{\text{cab}} + T_{\text{rec}}], \quad (18)$$

where  $G_{\text{im}}$  is the receiver image gain,  $F_{\text{eff}}$  the telescope forward efficiency,  $A = 1/\sin(\text{elevation})$  the airmass,  $\tau_s$  the atmospheric opacity in the signal band,  $T_{\text{atm}}$  the mean physical atmospheric temperature,  $T_{\text{cab}}$  the ambient temperature in the receiver cabine and  $T_{\text{rec}}$  the noise equivalent temperature of the receiver and the optics. All those parameters are easily measured, except  $\tau_s$ , which depends on the amount of water vapor in the atmosphere and which is estimated with complex atmospheric models.

The  $T_{\text{sys}}$  value is expressed so that all these terms are corrected for the attenuation by the atmosphere, the coupling of the antenna to the sky, and the side-band rejection. In other words, the system temperature is given in units that assume a perfect antenna (coupling equal to 1) located outside the atmosphere for a single-sideband signal.

### 4.2 Line vs continuum system temperature

Figure 1 shows the system temperature as a function of the radio frequency. The  $T_{\text{sys}}$  can vary significantly over the large bandwidth of the 2SB NOEMA receivers. Figure 3 shows the minimum and maximum system temperature inside the IF bandwidth for all possible local oscillator tunings. As a result, for continuum estimation, a frequency averaged  $T_{\text{sys}}$  is interpolated from a pre-computed table. The relevant frequency in that case is the LO frequency of the tuning (see Fig. 5). The averaging is done such as

$$\frac{1}{\langle T_{\text{sys}} \rangle^2} = \frac{1}{N} \sum \frac{1}{T_{\text{sys}}^2}. \quad (19)$$

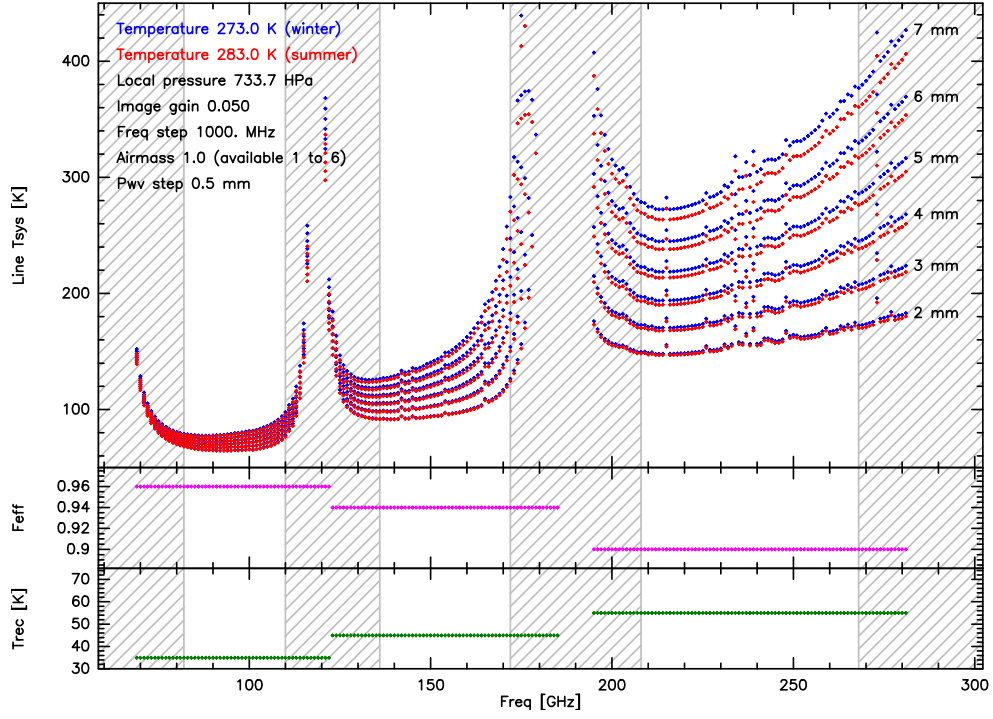


Figure 1: **Top:** Summer (red) and Winter (blue) semester  $T_{\text{sys}}$  for different precipitable water vapor (PWV) amount and for a source at zenith. The numbers indicate PWV values assumed in the computation. **Middle:** Assumed forward efficiencies in the computation. **Bottom:** Assumed receiver temperatures in the computation. This version is for the single band mode.

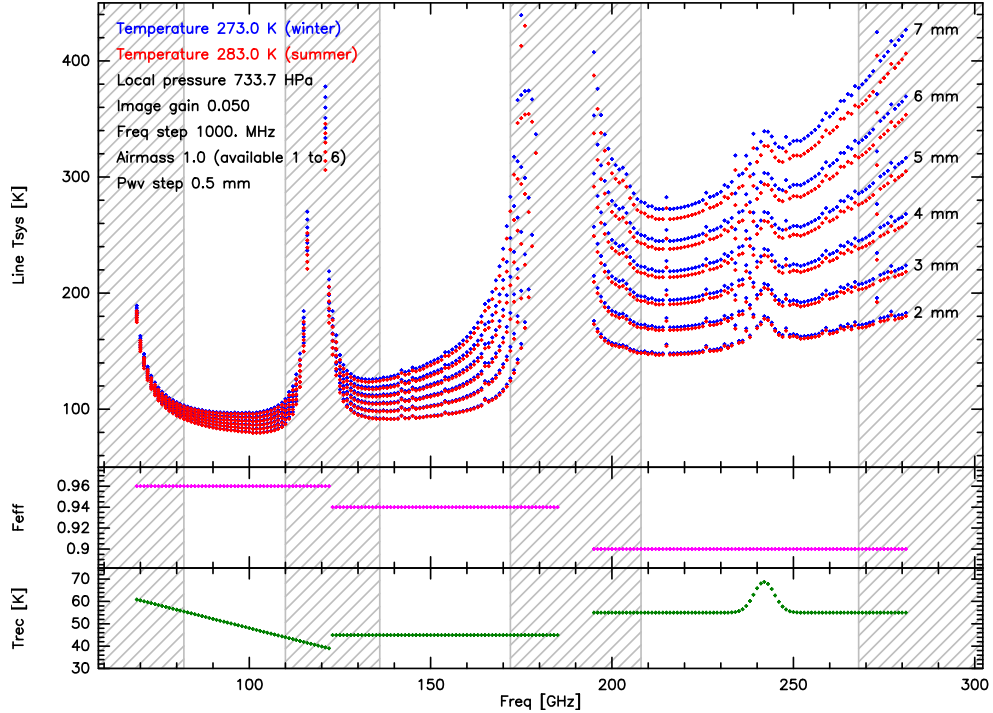


Figure 2: Same as Fig. 1, but for the dual band mode.



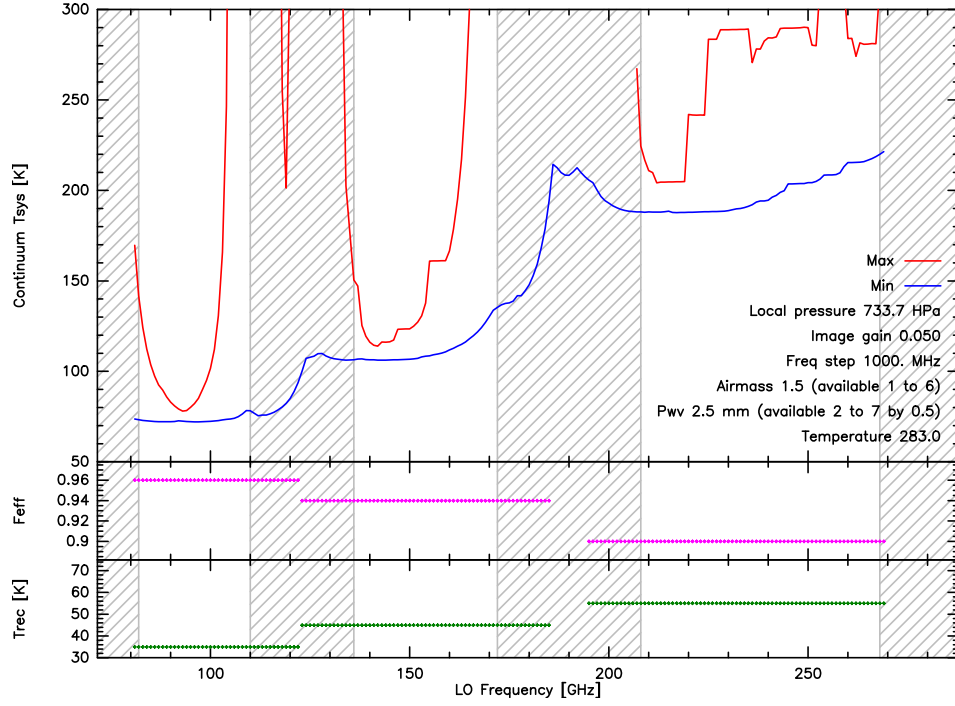


Figure 3: **Top:** Minimum and maximum  $T_{\text{sys}}$  obtained in the intermediate frequency bandwidth as a function of the local oscillator frequency used in the tuning. **Middle:** Assumed forward efficiencies in the computation. **Bottom:** Assumed receiver temperatures in the computation. This version is for the single band mode.

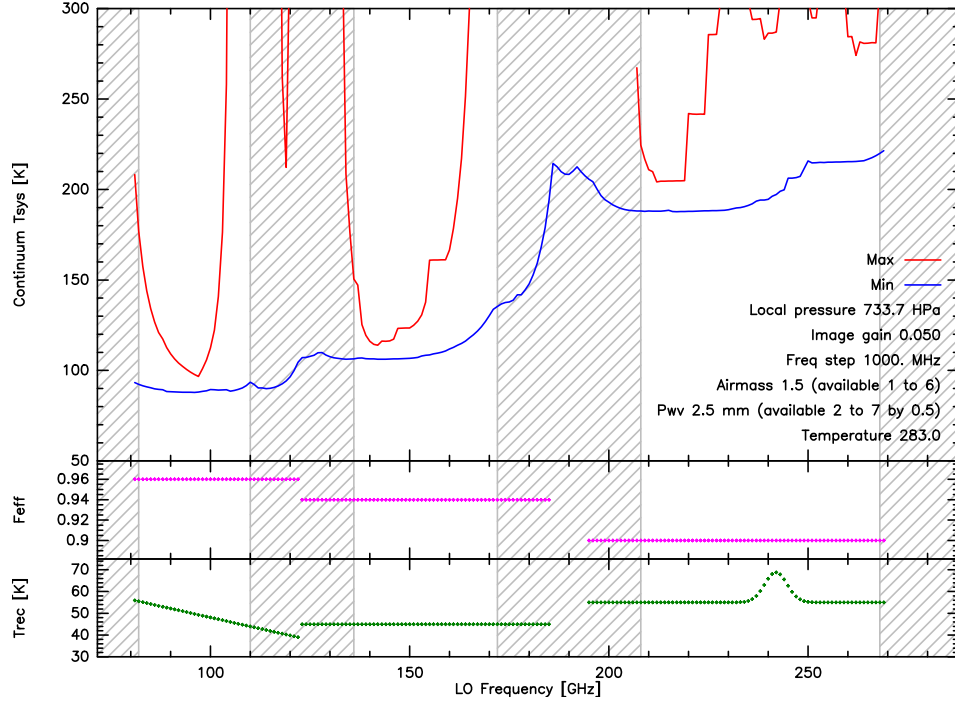


Figure 4: Same as Fig. 3, but for the dual band mode.

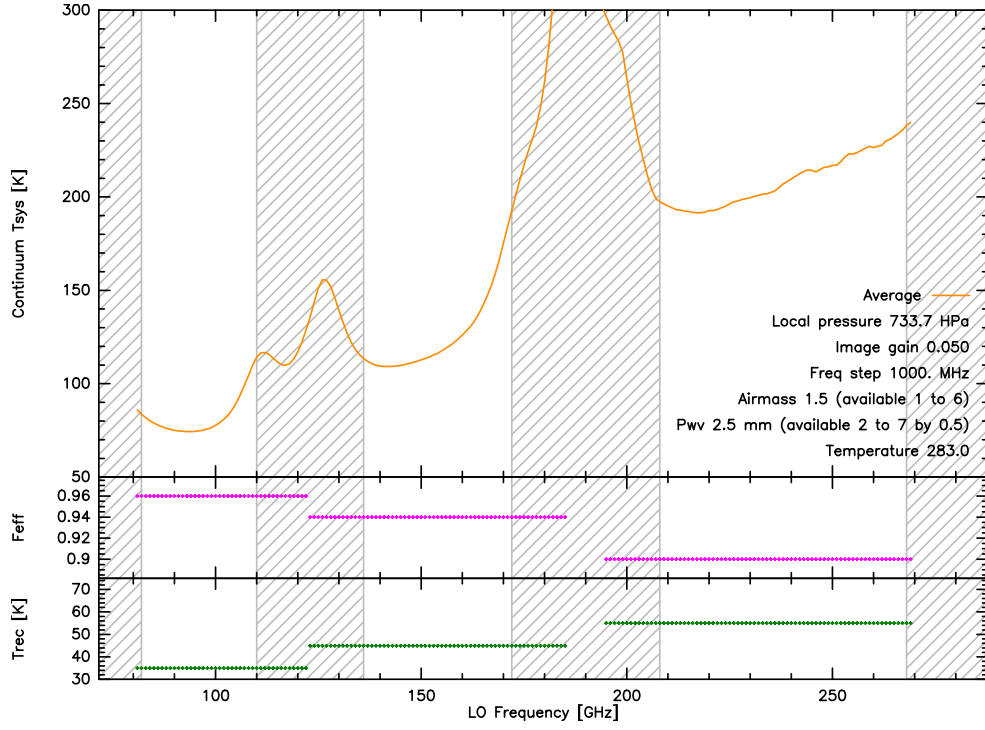


Figure 5: **Top:** Averaged “continuum”  $T_{\text{sys}}$  as a function of the local oscillator frequency used in the tuning. **Middle:** Assumed forward efficiencies in the computation. **Bottom:** Assumed receiver temperatures in the computation. This version is for the single band mode.

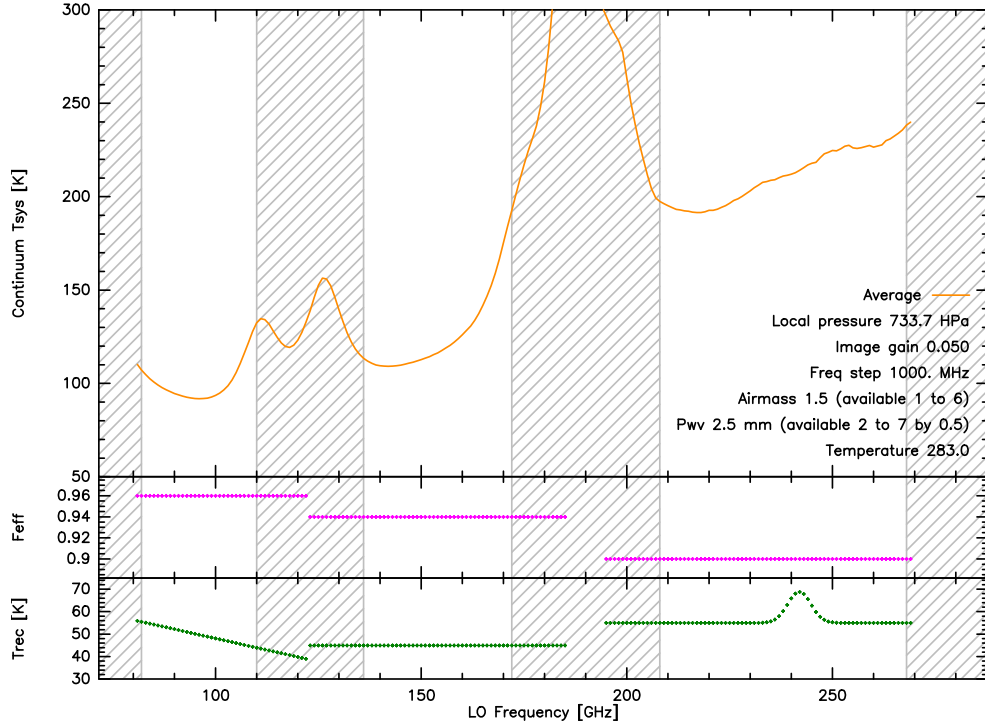


Figure 6: Same as Fig. 5, but for the dual band mode.

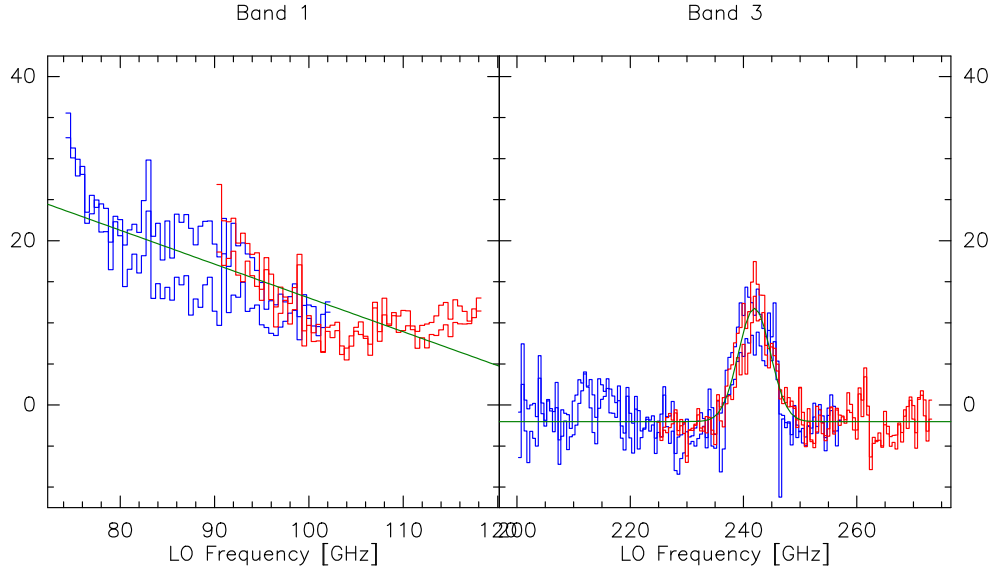


Figure 7: Fit of the receiver temperature added by the presence of the dual band dichroic on the optical path. The blue/red curves show the data for a LSB and USB LO tuning, respectively. The two curves per frequency and color show the measured results for the two polarizations.

### 4.3 Receiver temperature

The receiver temperature has two main contributions.

- The first one comes from the receiver when used in single band mode. The quality of current receivers and associated optics ensures that this one is to first order independent of the radio-frequency for each receiver, except at the edges of the receiver band. We thus model it as a constant receiver temperature per band. This contribution is shown on the bottom panels of Fig. 1 to 5.
- The second one comes from the dichroic that splits the beam as a function of the wavelength when in dual band mode. Figure 7 shows the variations of the dichroic receiver temperature as a function of the radio frequency. This contribution has a non-negligible contribution to the overall receiver temperature budget. We thus only add it when in dual band mode. Moreover it varies much as a function of the radio frequency. We thus model it as the sum of a linear contribution, plus a Gaussian centered around 240 GHz. This last bump corresponds to a physical phenomenon, named Wood anomaly, which occurs in the dichroic when it operates in reflection under oblique incidence.

## 5 In practice

### 5.1 Line vs continuum system temperature

In the online estimator (to be used for proposal preparation), the  $T_{\text{sys}}$  is interpolated in frequency, airmass, amount of precipitable water vapor, and ambient temperature from tabulated values (see Fig. 1). The airmass is estimated using the maximum elevation of a source at the chosen Declination. The values are different for summer and winter due to the different atmospheric characteristics. Moreover, the chosen amount of precipitable water vapor depends on the receiver band (in addition to the season) because the NOEMA operation team schedule the different receiver bands according to the actual weather (high frequency bands are scheduled only during the best weather conditions).

The system temperature for a given LO frequency can be computed using an atmospheric model in ASTRO (ASTRO\ATMOSPHERE command) with ambient temperature and precipitable water amount

as input. The overall computing time of the continuum system temperature would be prohibitive because of the computation of the atmospheric model over the  $2 \times 8$  GHz IF bandwidth sampled every 100 MHz. Instead the computation is done off-line on a grid of LO frequency sampled every 1 GHz.

## 5.2 The number of polarizations

All NOEMA antennas are equipped with dual polarization receivers. They measure the signal coming from the pointed direction in two perpendicular polarizations in the same frequency range. For the current generation of receiver (2006) and correlators, one or two polarizations are processed by the correlators, depending on the project settings. We thus have to introduce the number of polarizations  $n_{\text{pol}}$ , which can be set to 1 or 2 and insert it in the radiometer equation with

$$\sigma_{\text{Jy}} = \frac{J_{\text{ant}}^{\text{int}} T_{\text{sys}}}{\eta_{\text{spec}} \sqrt{n_{\text{ant}} (n_{\text{ant}} - 1)} d\nu n_{\text{pol}} \Delta t_{\text{on}}}. \quad (20)$$

## 5.3 Actual computations

The sensitivity estimator computes the relationship between  $\Delta t$  and  $\sigma_{\text{Jy}}$  with

$$\sigma_{\text{Jy}} = \frac{J_{\text{ant}}^{\text{int}} T_{\text{sys}}}{\eta_{\text{spec}} \sqrt{n_{\text{ant}} (n_{\text{ant}} - 1)} d\nu n_{\text{pol}} \Delta t_{\text{on}}} \quad \text{with} \quad J_{\text{ant}}^{\text{int}} = \frac{J_{\text{ant}}^{\text{sd}}}{\eta_{\text{atm}}} \quad \text{and} \quad \eta_{\text{atm}} = e^{-\frac{\phi_{\text{rms}}^2}{2}} \leq 1.0, \quad (21)$$

where  $T_{\text{sys}}$  is interpolated in frequency and airmass from the table, and the other parameters are defined by the observatory. It then computes the relationship between  $\sigma_{\text{K}}$  and  $\sigma_{\text{Jy}}$  with

$$\sigma_{\text{K}} = \frac{\sigma_{\text{Jy}}}{J_{\text{ant}}^{\text{syn}}} \quad \text{with} \quad J_{\text{ant}}^{\text{syn}} = \frac{2\pi k \theta_{\text{maj}} \theta_{\text{min}}}{4 \ln 2 \lambda^2}. \quad (22)$$

## 5.4 Elapsed telescope time vs on-source time

The goal of a sensitivity estimator is to find the rms noise obtained when observing during the elapsed telescope time,  $\Delta t_{\text{tel}}$ . The total integration time spent on-source  $\Delta t_{\text{on}}$  is shorter than the elapsed telescope time due to several factors. The actual on source time is then computed taking into account the following points:

1. **Instrumental setup time:** At the beginning of an observing track a significant time ( $\Delta t_{\text{setup}} \sim 40$  minutes according to history of observations) is spent in receiver tuning and calibration observations before observing the actual astronomical target. This means that even for a very short ON source time, a project cannot be shorter than  $\Delta t_{\text{setup}}$ . The setup time is computed as

$$\Delta t_{\text{setup}} = \Delta t_{\text{setupmin}} + (n_{\text{freq}} - 1) \Delta t_{\text{setup/freq}}, \quad (23)$$

where  $\Delta t_{\text{setupmin}}$  is the minimum setup time when only one frequency is observed (40 minutes),  $\Delta t_{\text{setup/freq}}$  is the additional setup time per additional frequency, and  $n_{\text{freq}}$  is the number of frequency observed in frequency cycling mode.  $\Delta t_{\text{setup/freq}}$  is for the moment also set to 40 minutes.

2. **Number of tracks per science goal:** Also, for long projects observed in several ( $n_{\text{track}}$ ) tracks the time spent for tuning and calibration is  $n_{\text{track}} \times \Delta t_{\text{setup}}$ . We thus define the time spent for observations (i.e. without instrumental setup)  $\Delta t_{\text{obs}}$  as:

$$\Delta t_{\text{obs}} = \Delta t_{\text{tel}} - n_{\text{track}} \times \Delta t_{\text{setup}}. \quad (24)$$

The number of tracks is computed as

$$n_{\text{track}} = \frac{\Delta t_{\text{tel}}}{\Delta t_{\text{visible}} + \Delta t_{\text{setup}}}, \quad (25)$$

where  $\Delta t_{\text{visible}}$  is the typical time when the source is visible from Bure, which depends on the source declination:

- Sources above 0 deg are observed 8 hours at most (for instrumental management),
- 8.2 hours for a declination of 0 deg (truncated to 8 hours),
- 6.5 hours for a declination of  $-10$  deg,
- 3.9 hours for a declination of  $-20$  deg,
- 0.0 hours for a declination of  $-30$  deg.
- Sources below  $-30$  deg can not be observed.

A linear interpolation with the declination is performed in the appropriate range between  $-30$  deg and  $0$  deg.

For short projects ( $\Delta t_{\text{tel}} < \Delta t_{\text{visible}} + \Delta t_{\text{setup}}$ ), the number of tracks  $n_{\text{track}}$  is set to 1. Otherwise, the floating value of  $n_{\text{track}}$  is used in the computation of  $\Delta t_{\text{obs}}$ . Since  $\Delta t_{\text{setup}}$  is constant whatever the length of a track the use of a floating value for  $n_{\text{track}}$  is somehow unnatural but it ensures that the conversion from  $\Delta t_{\text{tel}}$  to  $\Delta t_{\text{obs}}$  is a monotonic function, without regular threshold effects.

3. **Observing efficiency:** After the initial phase of instrumental setup, the observing mode does not dedicate 100% of the time to the astronomical target. Part of the time is spent for calibration (pointing, focus, atmospheric calibration,...) and to slew the telescopes between useful integrations. The time actually spent on source  $\Delta t_{\text{on}}$  is defined as

$$\Delta t_{\text{on}} = \Delta t_{\text{obs}} \times \eta_{\text{obs}} \quad (26)$$

where  $\eta_{\text{obs}} < 1.0$  is the observing efficiency. The exact computation of  $\eta_{\text{obs}}$  depends on the observing mode. The observing mode can be split into two categories that can be combined:

- Detection vs Imaging projects:** From the sensitivity estimation viewpoint, the main difference between these observing modes is the number of gain calibrators regularly observed:  $n_{\text{gaincal}} = 1$  for detection, and 2 for mapping projects.
- Frequency cycling mode:** In this case, the gain calibrators have to be observed at each frequency of the cycle.

These results in a computation of the observing efficiency as

$$\eta_{\text{obs}} = \frac{1}{\Omega_{\text{obs}}} \quad \text{with} \quad \Omega_{\text{obs}} = \Omega_{\text{min}} + n_{\text{gaincal}} n_{\text{freq}} \Omega_{\text{freq/gaincal}}, \quad \Omega_{\text{min}} = 1.3, \quad \text{and} \quad \Omega_{\text{freq/gaincal}} = 0.3. \quad (27)$$

Note that the exact value of  $\Omega_{\text{min}}$  and  $\Omega_{\text{freq/gaincal}}$  actually depend on several parameters such as the distance between the source and the calibrator(s). In “standard” mode, we obtain the usual  $\Omega_{\text{obs}} = 1.6$  and  $1.9$ , for detection and mapping projects, respectively. In frequency cycling mode with 2 frequencies, we yield  $\Omega_{\text{obs}} = 1.9$ , and  $2.5$  for detection and mapping projects, respectively.

4. **From  $\Delta t_{\text{obs}}$  to on-source time:** Finally, the distribution of observing time into the time spent on-source,  $\Delta t_{\text{on}}$ , actually used to estimate the sensitivity depends on three main observation kinds that are assumed exclusive from each other.

**Single-source, single-field observations** where the telescope tracks a single source during the full integration time. This mode is used when the signal-to-noise ratio is the limiting factor.

**Track-sharing, single-field observations** where the telescope regularly cycles between a few close-by sources. This mode is used when the sources are so bright that the limiting factor is the Earth synthesis, not the signal-to-noise ratio.

**Single-source mosaicking** where the telescope regularly cycles between close-by pointings that usually follows a hexagonal compact pattern whose side is  $\lambda/(2d_{\text{prim}})$ , where  $d_{\text{prim}}$  is the diameter of the interferometer antennas. This mode is used to image sources wider than the primary beam field of view.

In the following, we will work out the equations needed by the sensitivity estimator for each of these observing modes.

5. **Overall efficiency** Finally, the overall observing efficiency,  $\eta_{\text{tot}}$ , is evaluated by computing the sum of the on-source time over the total telescope time

$$\eta_{\text{tot}} = \frac{\Sigma \Delta t_{\text{on}}}{\Delta t_{\text{tel}}} \quad (28)$$

The sum of the on-source time allows us to take into account the fact that 1) the telescope time may be shared between sources or frequencies, and 2) dual band observations are more efficient than single band ones;. We also stress that when frequency cycling is combined with dual band observations, both receiver bands are affected by the efficiency loss of the frequency cycling even though one of the two bands could not require frequency cycling at all! A warning is raised when  $\eta_{\text{tot}} \leq 0.25$ .

## 5.5 Sensitivity for a single-source, single-field observations

That's the simplest case. The point source sensitivity in this case is

$$\sigma_{\text{Jy}} = \frac{J_{\text{ant}}^{\text{int}} T_{\text{sys}}}{\eta_{\text{spec}} \sqrt{n_{\text{ant}} (n_{\text{ant}} - 1) d\nu n_{\text{pol}} \Delta t_{\text{on}}}}, \quad (29)$$

where  $\Delta t_{\text{on}}$  is related to the total elapsed telescope time  $\Delta t_{\text{tel}}$  through

$$\Delta t_{\text{on}} = \eta_{\text{obs}} \eta_{\text{freq}} (\Delta t_{\text{tel}} - n_{\text{track}} \times \Delta t_{\text{setup}}), \quad (30)$$

where  $\eta_{\text{freq}}$  is the fraction of  $\Delta t_{\text{obs}}$  spent at one tuning frequency.  $\eta_{\text{freq}} = 1.0$  in “standard” mode and  $\eta_{\text{freq}} \sim 0.5$  when cycling between two frequencies. The sum of  $\eta_{\text{freq}}$  needs to equal 1.0!

## 5.6 Sensitivity for track-sharing, single-field observations

In this case, the telescope time is equally divided between the  $n_{\text{sou}}$  observed sources. This yields

$$\sigma_{\text{Jy}} = \frac{J_{\text{ant}}^{\text{int}} T_{\text{sys}}}{\eta_{\text{spec}} \sqrt{n_{\text{ant}} (n_{\text{ant}} - 1) d\nu n_{\text{pol}} \Delta t_{\text{on}}}} \quad (31)$$

$$\text{with } \Delta t_{\text{on}} = \eta_{\text{obs}} \eta_{\text{freq}} \left( \frac{\Delta t_{\text{tel}} - n_{\text{track}} \times \Delta t_{\text{setup}}}{n_{\text{sou}}} \right). \quad (32)$$

While it is technically feasible to observe sources in track-sharing with different integration times, this case is not implemented (yet) in the sensitivity estimator, and the different sensitivities should be computed independently.

## 5.7 Sensitivity for mosaicking

Note: No provision is made to estimate the sensitivity of a mosaic in frequency cycling mode. This is to avoid mixing the complexity of both modes...

Mosaicking is a particular case of wide-field imaging: The user wishes to observe a given field of view larger than the primary beam size with a sensitivity as uniform as possible. The targeted field (which area is  $A_{\text{map}}$ , define by the user) can be divided in a number of independent resolution elements or independent (primary) beams  $n_{\text{beam}}$ . We have:

$$n_{\text{beam}} = \frac{A_{\text{map}}}{A_{\text{beam}}} \quad (33)$$

where  $A_{\text{beam}}$  is the area of the primary beam. It is linked to the telescope full width at half maximum ( $\theta$ ) by

$$A_{\text{beam}} = \frac{0.8 \pi \theta_{\text{prim}}^2}{4 \ln(2)}, \quad (34)$$

The 0.8 factor represents the truncation of the beam at 20% of its maximum, which is performed during the imaging process.

For the sensitivity estimation we assume a standard sampling of targeted field and the on-source time is equally divided between the independent primary beams  $n_{\text{beam}}$  in the targeted field of view. We thus yield at the center of a Nyquist sampled mosaic

$$\sigma_{\text{Jy}} = \frac{J_{\text{ant}}^{\text{int}} T_{\text{sys}}}{\eta_{\text{spec}} \sqrt{n_{\text{ant}} (n_{\text{ant}} - 1) d\nu n_{\text{pol}} \Delta t_{\text{on}}}} \quad (35)$$

$$\text{with } \Delta t_{\text{on}} = \eta_{\text{obs}} \eta_{\text{mos}} \left( \frac{\Delta t_{\text{tel}} - n_{\text{track}} \times \Delta t_{\text{setup}}}{n_{\text{beam}}} \right), \quad \text{and} \quad \eta_{\text{mos}} = \frac{\Delta t_{\text{point/cycle}}}{\Delta t_{\text{point/cycle}} + \Delta t_{\text{slew}}}, \quad (36)$$

where where  $\Delta t_{\text{point/cycle}}$  is the integration time per pointing during each single mosaic cycle, and  $\Delta t_{\text{slew}}$  is the time to slew between two consecutive pointings. There are several subtleties in these computations.

- $A_{\text{map}}$  **must be larger than 2 times**  $A_{\text{beam}}$ . Below this we advise to use the track sharing mode with two independent fields.
- **Eq. 59 is only valid at the center of a mosaic, not at its edges!** Indeed, the processing (imaging and deconvolution) of a mosaic implies a division by the primary beam of the interferometer. As the primary beam is to first order a Gaussian decreasing to zero, this implies that the noise of the mosaic will vary over the field of view. In particular it increases sharply at the edges of the field of view.
- **In these equations,  $n_{\text{beam}}$  is smaller than  $n_{\text{point}}$ , the number of pointed positions that are observed in the mosaic.** The cycling of the pointings of the mosaic should ensure Nyquist sampling of the observed field of view. This implies that there is an important redundancy between the pointings, contrary to track sharing where the sources are supposed to be fully independent on the sky. For instance, when mosaicking with a hexagonal compact pattern, each line of sight will be observed by 7 contiguous pointings, except at the mosaic edges. It can thus been shown that the number of mosaic pointings,  $n_{\text{point}}$ , is related to the number of independent elements through

$$n_{\text{point}} = n_{\text{beam}} \left( \frac{7}{4} \right)^2, \quad (37)$$

for a correctly sampled mosaic. **Equation 59 is thus only valid inside a correctly sampled mosaic.**

- **Degradation of the observing efficiency** The pointings of a mosaic must be observed in relatively short time cycles to ensure that all pointings are observed with similar weather conditions and that they share similar  $uv$  coverage. This will minimize the shift-variant part of the interferometer wide-field imaging response. This calls for the shortest possible integration time per pointing. However, the interferometer takes time to slew from one pointing to the next one without integrating. As a result, the observing efficiency  $\eta_{\text{obs}}$  is degraded in the cases of mosaics. We model it as a mosaic efficiency factor,  $\eta_{\text{mos}}$ . Having a large integration time per pointing during one cycle compared to  $\Delta t_{\text{slew}}$  will decrease the mosaicking overhead. This requirement is in sharp contrast with the previous one, namely the need to homogenize the interferometer wide-field response. The best compromise comes from two different considerations.

1. The smallest integration time per scan is set by the acquisition system (for instance, the maximum achievable data rate). In practice, we enforce that

$$\Delta t_{\text{min}} \leq \Delta t_{\text{int/scan}} \quad \text{with} \quad \Delta t_{\text{min}} = 10 \text{ sec.} \quad (38)$$

2. The distance covered by a visibility in the  $uv$ -plane during an integration should always smaller than the distance associated to tolerable aliasing (see Pety and Rodríguez-Fernández 2010 for more details). This can be written as the following condition (Eq. C.3 in this article)

$$\frac{\Delta t_{\text{int/scan}}}{1 \text{ s}} << \frac{6900}{\theta_{\text{alias}}/\theta_{\text{syn}}}, \quad (39)$$

where  $\theta_{\text{alias}}$  is the map angular size, and  $\theta_{\text{syn}}$  the angular resolution. For a given angular resolution, the interferometer minimum integration time corresponds to

$$\Delta t_{\text{int/scan}} \leq \eta \frac{6900}{1 \text{ sec}} \sqrt{\frac{\theta_{\text{maj}}\theta_{\text{min}}}{A_{\text{map}}}}, \quad (40)$$

where  $\eta$  is a **ad-hoc number set to 0.5** to ensure that the condition defined in Eq. 39 is met.

3. For operational reasons, the duration of a scan is limited to 45 sec.
4. In summary,

$$10 \text{ sec} \leq \Delta t_{\text{int/scan}} = \min \left( 45 \text{ sec}, \eta \frac{6900}{1 \text{ sec}} \sqrt{\frac{\theta_{\text{maj}}\theta_{\text{min}}}{A_{\text{map}}}} \right) \quad \text{with} \quad \eta = 0.5. \quad (41)$$

As the typical slew time between two pointings is  $\Delta t_{\text{slew}} = 11 \text{ sec}$ , we yield that

$$0.47 \leq \eta_{\text{mos}} \leq 1.0. \quad (42)$$

- **Improving the observing efficiency for small mosaics** In A configuration, the integration time per scan should be less than 22 sec to meet the criteria of Eq. 39. However, this implies a mosaic efficiency of only  $\eta_{\text{mos}} = 0.67$ ! It is possible to greatly increase this efficiency for small mosaics by observing several time the same pointing in time-contiguous scans. Let's assume that we use an integration time of  $\Delta t_{\text{min}}$  per scan, and that we repeat it  $n_{\text{repeat/point/cycle}}$  before slewing to another pointing position. This gives

$$\eta_{\text{mos}} = \frac{\Delta t_{\text{point/cycle}}}{\Delta t_{\text{point/cycle}} + \Delta t_{\text{slew}}} \quad \text{and} \quad \Delta t_{\text{cycle}} = n_{\text{point/track}} (\Delta t_{\text{point/cycle}} + \Delta t_{\text{slew}}), \quad (43)$$

with

$$\Delta t_{\text{point/cycle}} = n_{\text{repeat/point/cycle}} \Delta t_{\text{int/scan}}. \quad (44)$$



As stated above, we wish to cycle as quickly as possible through the different pointings in a single cycle to homogenize the observing conditions over the mosaic. This implies to introduce a maximum time to cycle all the mosaic pointings. Let's assume that we want to homogenize the conditions during the maximum time allowed between two gain calibrations, ie.,  $\Delta t_{\text{calmax}} = 25$  min. This yields the maximum number of repeats per pointing and per cycle and thus the mosaic efficiency as

$$n_{\text{repeat/point/cycle}}^{\text{max}} = \frac{\Delta t_{\text{calmax}}/n_{\text{point/track}} - \Delta t_{\text{slew}}}{\Delta t_{\text{int/scan}}}, \quad \text{and} \quad \eta_{\text{mos}} = 1 - \frac{n_{\text{point/track}} \Delta t_{\text{slew}}}{\Delta t_{\text{calmax}}}. \quad (45)$$

The maximum number of repeats must be larger than 1. This sets the limit in number of pointings per track between small and large mosaics.

$$n_{\text{point/track}}^{\text{large}} = \text{floor} \left( \frac{\Delta t_{\text{calmax}}}{\Delta t_{\text{int/scan}} + \Delta t_{\text{slew}}} \right). \quad (46)$$

- **Checking the feasibility of a large mosaic** For large mosaics, it is advised to cycle all the pointings of a given mosaic in less than 1 hour. This ensures that the uv plane will be sampled at least 8 times per standard track of 8 hours. Setting the maximum time to cycle all the pointings,  $\Delta t_{\text{cyclemax}}$ , to 60 minutes, we yield that the maximum number of pointing per track is

$$n_{\text{point/track}}^{\text{max}} = \frac{\Delta t_{\text{cyclemax}}}{\Delta t_{\text{min}} + \Delta t_{\text{slew}}} \sim 150. \quad (47)$$

Hence, if the PI wishes to observe an area that will require more that 150 pointings per independent track, the estimator will ask to either increase the requested elapsed telescope time or to decrease the requested field-of-view area.

Moreover, we need to adapt the optimal integration time per scan to ensure that all pointings per track will be cycled in  $\Delta t_{\text{cyclemax}}$ . This gives

$$\Delta t_{\text{int/scan}} = \min \left\{ \Delta t_{\text{int/scan}}, \left( \frac{\Delta t_{\text{cyclemax}}}{n_{\text{point/track}}} - \Delta t_{\text{slew}} \right) \right\}. \quad (48)$$

In the case of large mosaics, the minimum mosaic efficiency is

$$\eta_{\text{min}} = \frac{\Delta t_{\text{min}}}{\Delta t_{\text{min}} + \Delta t_{\text{slew}}} = 0.47. \quad (49)$$

In summary, correctly setting up the sensitivity estimate for a mosaic requires

1. To compute the number of independent primary beams in the targeted field of view

$$n_{\text{beam}} = \frac{A_{\text{map}}}{A_{\text{beam}}}, \quad \text{where} \quad A_{\text{beam}} = \frac{0.8 \pi \theta_{\text{prim}}^2}{4 \ln(2)}. \quad (50)$$

2. To compute the number of pointings in the mosaic and the number of pointings per track

$$n_{\text{point}} = n_{\text{beam}} \left( \frac{7}{4} \right)^2, \quad \text{and} \quad n_{\text{point/track}} = \min \left( n_{\text{point}}, \frac{n_{\text{point}}}{n_{\text{track}}} \right). \quad (51)$$

3. To compute the optimal integration time per scan with

$$10 \text{ sec} \leq \Delta t_{\text{int/scan}} = \min \left( 45 \text{ sec}, \eta \frac{6900}{1 \text{ sec}} \sqrt{\frac{\theta_{\text{maj}} \theta_{\text{min}}}{A_{\text{map}}}} \right) \quad \text{with} \quad \eta = 0.5. \quad (52)$$

The minimum integration time per scan of 10 seconds implies the maximum dynamic of scales that can be observed in a single track.

4. To compute the number of points per track that define the limit between small and large mosaics with

$$n_{\text{point/track}}^{\text{large}} = \text{floor} \left( \frac{\Delta t_{\text{calmax}}}{\Delta t_{\text{int/scan}} + \Delta t_{\text{slew}}} \right), \quad \text{where} \quad \Delta t_{\text{slew}} = 11 \text{ sec}, \quad \text{and} \quad \Delta t_{\text{calmax}} = 25 \text{ min.} \quad (53)$$

5. To compute the maximum number of repeats per pointing and per cycle, depending on the mosaic size.

- For a small mosaic ( $n_{\text{point/track}} \leq n_{\text{point/track}}^{\text{large}}$ ), it is

$$n_{\text{repeat/point/cycle}}^{\text{max}} = \frac{\frac{\Delta t_{\text{calmax}}}{n_{\text{point/track}}} - \Delta t_{\text{slew}}}{\Delta t_{\text{int/scan}}}. \quad (54)$$

- For a large mosaic ( $n_{\text{point/track}} > n_{\text{point/track}}^{\text{large}}$ ), it is just set to  $n_{\text{repeat/point/cycle}}^{\text{max}} = 1$ .

6. To check that the maximum number of pointings per track is not yet reached with

$$n_{\text{point/track}} \leq n_{\text{point/track}}^{\text{max}}, \quad \text{where} \quad n_{\text{point/track}}^{\text{max}} = \frac{\Delta t_{\text{cyclemax}}}{\Delta t_{\text{min}} + \Delta t_{\text{slew}}} \sim 150, \quad \text{and} \quad \Delta t_{\text{cyclemax}} = 60 \text{ min.} \quad (55)$$

If the PI wishes to observe an area that will require more that 150 pointings per independent track, the estimator will ask to either increase the requested elapsed telescope time or to decrease the requested field-of-view area.

7. To adapt the optimal integration time per scan to ensure that all pointings per track will be cycled in  $\Delta t_{\text{cyclemax}}$  **only for a large mosaic** with

$$\text{if } n_{\text{point/track}} > n_{\text{point/track}}^{\text{large}}, \quad \text{then} \quad \Delta t_{\text{int/scan}} = \min \left\{ \Delta t_{\text{int/scan}}, \left( \frac{\Delta t_{\text{cyclemax}}}{n_{\text{point/track}}} - \Delta t_{\text{slew}} \right) \right\}. \quad (56)$$

8. To compute the actual mosaic efficiency and time to complete a full cycle with

$$\eta_{\text{mos}} = \frac{\Delta t_{\text{point/cycle}}}{\Delta t_{\text{point/cycle}} + \Delta t_{\text{slew}}}, \quad \text{and} \quad \Delta t_{\text{point/cycle}} = n_{\text{repeat/point/cycle}}^{\text{max}} \Delta t_{\text{int/scan}}, \quad (57)$$

and

$$\Delta t_{\text{cycle}} = n_{\text{point/track}} (\Delta t_{\text{point/cycle}} + \Delta t_{\text{slew}}). \quad (58)$$

These two quantities should be given as feedback to the user.

9. To finally compute the sensitivity with

$$\sigma_{\text{Jy}} = \frac{J_{\text{ant}}^{\text{int}} T_{\text{sys}}}{\eta_{\text{spec}} \sqrt{n_{\text{ant}} (n_{\text{ant}} - 1) d\nu n_{\text{pol}} \Delta t_{\text{on}}}}, \quad \text{and} \quad \Delta t_{\text{on}} = \eta_{\text{obs}} \eta_{\text{mos}} \left( \frac{\Delta t_{\text{tel}} - n_{\text{track}} \times \Delta t_{\text{setup}}}{n_{\text{beam}}} \right). \quad (59)$$

## 6 Acknowledgements

We thank Anne-Laure Fontana for providing us in advance with the receiver temperature measurements with and without dichroics.

## References

Kraus, J. D., in McGraw-Hill 1982 (1966), Radio Astronomy.

## A A few reminders: Flux vs brightness in radio-astronomy

### A.1 Antenna power pattern, solid angles, associated efficiencies

The power pattern,  $P_{\text{ant}}(\theta, \phi, \nu)$ , is a measure of the response of the antenna to radiation as a function of the angles  $\theta$  and  $\phi$ . It is a normalized (maximum value unity), dimensionless quantity. It can depend on the frequency of observation.

The beam area or beam solid angle (or pattern solid angle) is

$$\Omega_{\text{ant}}(\nu) = \iint_{4\pi} P_{\text{ant}}(\theta, \phi, \nu) d\Omega, \quad (60)$$

where

$\Omega_{\text{ant}}$	[sr]	beam area,
$P_{\text{ant}}$	[dimensionless]	normalized power pattern of antenna,
$d\Omega$	[sr]	infinitesimal solid angle of sky ( $= \sin \theta d\theta d\phi$ ).

The forward beam and main beam solid angles are the integral of the power pattern over  $2\pi$  and the main lobe, respectively, i.e.,

$$\Omega_{\text{fb}}(\nu) = \iint_{2\pi} P_{\text{ant}}(\theta, \phi, \nu) d\Omega, \quad \text{and} \quad \Omega_{\text{mb}}(\nu) = \iint_{\text{main lobe}} P_{\text{ant}}(\theta, \phi, \nu) d\Omega. \quad (61)$$

The forward and beam efficiencies are then defined as

$$F_{\text{eff}} = \frac{\Omega_{\text{fb}}}{\Omega_{\text{ant}}}, \quad \text{and} \quad B_{\text{eff}} = \frac{\Omega_{\text{mb}}}{\Omega_{\text{ant}}}. \quad (62)$$

### A.2 Source and observed flux density

The integral of the brightness over the source extension yields the total source flux density

$$F_{\text{sou}}(\nu) = \iint_{\text{source}} B(\theta, \phi, \nu) d\Omega, \quad (63)$$

where

$F_{\text{sou}}$	[W m <sup>-2</sup> Hz <sup>-1</sup> ]	flux density of source,
$B$	[W m <sup>-2</sup> Hz <sup>-1</sup> sr <sup>-1</sup> ]	brightness as a function of position over source,
$d\Omega$	[sr]	infinitesimal solid angle of sky ( $= \sin \theta d\theta d\phi$ ).

When the source is observed with an antenna of power pattern ( $P_{\text{ant}}$ ), the observed flux density in direction  $(\theta_0, \phi_0)$  is

$$F_{\text{obs}}(\theta_0, \phi_0, \nu) = \iint_{\text{source}} B(\theta, \phi, \nu) P_{\text{ant}}(\theta - \theta_0, \phi - \phi_0, \nu) d\Omega, \quad (64)$$

where

This integral is a correlation. We now introduce the mirror symmetric of the antenna pattern to yield a convolution

$$F_{\text{obs}}(\theta_0, \phi_0, \nu) = \iint_{\text{source}} B(\theta, \phi, \nu) \tilde{P}_{\text{ant}}(\theta_0 - \theta, \phi_0 - \phi, \nu) d\Omega, \quad (65)$$

$$\text{where } \tilde{P}_{\text{ant}}(\theta_0 - \theta, \phi_0 - \phi, \nu) = P_{\text{ant}}(\theta - \theta_0, \phi - \phi_0, \nu). \quad (66)$$

The distinction of these two patterns is only important for non-axisymmetrical cases.

$F_{\text{obs}}(\theta_0, \phi_0)$	$[\text{W m}^{-2} \text{Hz}^{-1}]$	observed flux density,
$B$	$[\text{W m}^{-2} \text{Hz}^{-1} \text{sr}^{-1}]$	brightness as a function of position over source,
$P_{\text{ant}}$	[dimensionless]	normalized antenna power pattern,
$d\Omega$	[sr]	infinitesimal solid angle of sky ( $= \sin \theta d\theta d\phi$ ).

### A.3 Observed brightnesses

The brightness observed in direction  $(\theta_0, \phi_0)$  is the flux density observed in this direction divided by the typical beam area

$$B_{\text{obs}}(\theta_0, \phi_0, \nu) = \frac{1}{\Omega} \iint_{\text{source}} B(\theta, \phi, \nu) \tilde{P}_{\text{ant}}(\theta_0 - \theta, \phi_0 - \phi, \nu) d\Omega, \quad (67)$$

where

$B_{\text{obs}}(\theta_0, \phi_0)$	$[\text{W m}^{-2} \text{Hz}^{-1} \text{sr}^{-1}]$	<b>observed</b> brightness,
$B$	$[\text{W m}^{-2} \text{Hz}^{-1} \text{sr}^{-1}]$	<b>actual</b> brightness as a function of position over source,
$\Omega$	[sr]	typical beam area,
$P_{\text{ant}}$	[dimensionless]	normalized antenna power pattern,
$d\Omega$	[sr]	infinitesimal solid angle of sky ( $= \sin \theta d\theta d\phi$ ).

The **typical** beam area is an ambiguous notion. Indeed, there are three different solid angles that can be used in this formula: The antenna beam solid angle ( $\Omega_{\text{ant}}$ ), the forward beam solid angle ( $\Omega_{\text{fb}}$ ), or the main beam solid angle ( $\Omega_{\text{mb}}$ )

$$B_{\text{ant}}(\theta_0, \phi_0, \nu) = \frac{1}{\Omega_{\text{ant}}} \iint_{\text{source}} B(\theta, \phi, \nu) \tilde{P}_{\text{ant}}(\theta_0 - \theta, \phi_0 - \phi, \nu) d\Omega, \quad (68)$$

$$B_{\text{fb}}(\theta_0, \phi_0, \nu) = \frac{1}{\Omega_{\text{fb}}} \iint_{\text{source}} B(\theta, \phi, \nu) \tilde{P}_{\text{ant}}(\theta_0 - \theta, \phi_0 - \phi, \nu) d\Omega, \quad (69)$$

$$\text{and } B_{\text{mb}}(\theta_0, \phi_0, \nu) = \frac{1}{\Omega_{\text{mb}}} \iint_{\text{source}} B(\theta, \phi, \nu) \tilde{P}_{\text{ant}}(\theta_0 - \theta, \phi_0 - \phi, \nu) d\Omega. \quad (70)$$

It is trivial to show that

$$B_{\text{fb}} = \frac{1}{F_{\text{eff}}} B_{\text{ant}} \quad \text{and} \quad B_{\text{mb}} = \frac{F_{\text{eff}}}{B_{\text{eff}}} B_{\text{fb}}. \quad (71)$$

At IRAM, the observed brightness obtained after a single-dish calibration are by default computed using the forward beam solid angle.

### A.4 Basic relation between received spectral power and sky brightness

The spectral power (infinitesimal power per unit frequency bandwidth) received from a solid angle of the sky on a surface of area is

$$dw(\theta, \phi, \nu) = B(\theta, \phi, \nu) \cos \theta d\Omega dA, \quad (72)$$

where

### A.5 Brightness temperature

#### A.5.1 Brightness temperature

In 1928, Nyquist showed that the noise power per unit bandwidth produced by a resistor of resistance,  $R$ , and physical temperature,  $T$ , is

$$dw = kT. \quad (73)$$

$dw$	$[\text{W Hz}^{-1}]$	spectral power,
$\theta$	$[\text{rad}]$	angle between $d\Omega$ and Zenith,
$\phi$	$[\text{rad}]$	angle between $d\Omega$ and East,
$\nu$	$[\text{Hz}]$	frequency of observation,
$B$	$[\text{W m}^{-2} \text{ Hz}^{-1} \text{ sr}^{-1}]$	sky brightness at position $(\theta, \phi)$ and frequency $\nu$ ,
$d\Omega$	$[\text{sr}]$	infinitesimal solid angle of sky $(= \sin \theta d\theta d\phi)$ ,
$dA$	$[\text{m}^2]$	infinitesimal surface area.

This relationship indicates that any spectral power can be expressed as a temperature using this relationship. For instance, the observed main beam temperature is defined as

$$T_{\text{mb}}(\theta_0, \phi_0, \nu) = \frac{1}{\Omega_{\text{mb}}} \iint_{\text{source}} B(\theta, \phi, \nu) \tilde{P}_{\text{ant}}(\theta_0 - \theta, \phi_0 - \phi, \nu) d\Omega. \quad (74)$$

### A.5.2 Interpretation

It happens that when an astronomical source, whose angular extent fills exactly the main lobe, emits as a black-body in the Rayleigh-Jeans regime ( $h\nu \ll kT$ ), the main-beam temperature is directly the physical temperature of the emitting source. However, this interpretation is only valid when the stated conditions are met. This almost never happens in (sub)-millimeter radio-astronomy because the emitting sources are often out of local thermodynamic equilibrium and  $h\nu \sim kT$ . So this interpretation is mostly misleading for newcomers.

As the measured spectral power in radio-astronomy have very small values, it is easier to express them in term of temperatures that will be orders of magnitude larger because  $k = 1.380658 \times 10^{23} \text{ J K}^{-1}$ . As a matter of fact, most observed brightness temperatures have values close to 1 (within a factor 1000!)

So it's easier to interpret the above relationship as: expressing spectral powers in terms of temperature is just a useful convenience.

## A.6 Effective aperture and aperture efficiency

Let's define the effective aperture of an antenna,  $A_{\text{eff}}$ , through the relationship between the received spectral power and the sky brightness

$$dw(\theta_0, \phi_0, \nu) = \frac{1}{2} A_{\text{eff}} \iint_{\text{source}} B(\theta, \phi, \nu) \tilde{P}_{\text{ant}}(\theta_0 - \theta, \phi_0 - \phi, \nu) d\Omega. \quad (75)$$

This definition is based on Eq. 72 with the assumption that the power pattern is independent of infinitesimal surface area of the receiving antenna in order to be able to factorize the integral on this infinitesimal surface area. Moreover the factor  $1/2$  corresponds to the case where the radiation is incoherent and unpolarized, and the receiver is only sensitive to one polarization.

This effective aperture corresponds to the fraction of the power density of a plane wave that is intercepted by the antenna. It has the unit of a surface  $[\text{m}^2]$ . It thus resembles a cross-section in particle physics. We thus define the aperture efficiency,  $\eta_{\text{ant}}$ , as the ratio of the effective aperture by the geometric aperture of the antenna

$$\eta_{\text{ant}} = \frac{A_{\text{eff}}}{A_{\text{geo}}} < 1, \quad \text{where} \quad A_{\text{geo}} = \pi \left( \frac{D_{\text{ant}}}{2} \right)^2. \quad (76)$$

## A.7 Relationship between effective aperture and antenna solid angle

### A.7.1 Statement

An important relationship in antenna theory is

$$\boxed{A_{\text{eff}}(\nu) \Omega_{\text{ant}}(\nu) = \lambda^2,} \quad (77)$$

where  $\lambda$  is the observed wavelength.

### A.7.2 Demonstration

A generic demonstration of this statement uses a thought experiment. Let's assume that the antenna is put in a box at a given physical temperature,  $T$ . This box can be considered an emitting black-body. If the frequency is appropriately chosen, the Rayleigh-Jeans regime is fulfilled. This implies that the source brightness is

$$B(\theta, \phi, \nu) = \frac{2kT}{\lambda^2}, \quad (78)$$

and the observed spectral power is

$$dw(\theta_0, \phi_0, \nu) = \frac{1}{2} A_{\text{eff}} \iint_{\text{source}} B(\theta, \phi, \nu) \tilde{P}_{\text{ant}}(\theta_0 - \theta, \phi_0 - \phi, \nu) d\Omega = \frac{1}{2} A_{\text{eff}} \Omega_{\text{ant}}(\nu) \frac{2kT}{\lambda^2}. \quad (79)$$

If we plug a matched resistor at the antenna output, it will deliver a noise power of

$$dw(\theta_0, \phi_0, \nu) = kT, \quad (80)$$

because its temperature is  $T$ . As it is matched to the antenna, this power is also the spectral power measured by the antenna. Hence, equating the last two equations, we yield the searched relationship.

### A.7.3 Interpretation

While this relationship was derived using a particular experimental setup, it yields a result that only characterize the state of the antenna. As usual in thermodynamics, the state is independent on the exact setup. This implies that the relationship is valid independent on the way it was yielded.

Nevertheless the demonstration is useful to understand that the solid angle that we have to consider in this relationship is the beam area, i.e., the coupling of the antenna to all direction in  $4\pi \text{ sr}$ . It is then possible to rewrite this relationship as

$$\boxed{A_{\text{eff}}(\nu) \Omega_{\text{fb}}(\nu) = \lambda^2 F_{\text{eff}}(\nu) \quad \text{and} \quad A_{\text{eff}}(\nu) \Omega_{\text{mb}}(\nu) = \lambda^2 B_{\text{eff}}(\nu).} \quad (81)$$

Using the definition of the aperture efficiency, we yield

$$B_{\text{eff}}(\nu) = \eta_{\text{ant}} A_{\text{geo}} \frac{\Omega_{\text{mb}}(\nu)}{\lambda^2}. \quad (82)$$

As

$$A_{\text{geo}} = \frac{\pi}{4} D^2, \quad \frac{\Omega_{\text{mb}}(\nu)}{\lambda^2} = \frac{\pi}{4 \ln 2} \left( \frac{\theta_{\text{mb}}}{\lambda} \right)^2, \quad \text{and} \quad \theta_{\text{mb}} = \alpha \frac{\lambda}{D}, \quad (83)$$

we yield

$$\boxed{B_{\text{eff}}(\nu) = \frac{\pi^2}{16 \ln 2} \alpha^2 \eta_{\text{ant}}(\nu) \simeq 0.8899 \alpha^2 \eta_{\text{ant}}(\nu).} \quad (84)$$

The factor  $\alpha$  defines the coupling of the optics to the sky, which can be computed with Gaussian optics. Its value is typically  $\alpha \sim 1.2$ . Finally, the Ruze theory indicates that the aperture efficiency is linked to the RMS ( $\sigma$ ) of the deviation of the telescope surface to a perfect parabola as

$$\boxed{\eta_{\text{ant}}(\nu) = \eta_{\text{ant}}^0 \exp \left\{ - \left( \frac{4\pi\sigma}{\lambda} \right)^2 \right\}.} \quad (85)$$